Using Recycled Materials in a Novel Dual Binder System for Hard Carbon Anodes: Closing the Loop Toward Sustainable Li-/Na-ion Batteries

ADVANCED FUNCTIONAL MATERIALS
www.afm-journal.de

Using Recycled Materials in a Novel Dual Binder System for Hard Carbon Anodes: Closing the Loop Toward Sustainable Li-/Na-ion Batteries

Hamideh Darjazi, Alessandro Piovano, Giuseppina Meligrana, Giuseppe A. Elia, and Claudio Gerbaldi**

Hard carbon (HC) has significant potential as anode material for both Li-ion and Na-ion batteries; however, its commercialization is hindered by challenges such as poor rate capability and low initial Coulombic efficiency (ICE). Although polymeric binders constitute a small fraction of the overall electrode composition, they play a crucial role in influencing the electrochemical performance. Here, this study introduces a novel dual composite binder, combining polyacrylic acid (PAA) and polyvinyl butyral (PVB). The interaction between the COOH groups in PAA and the OH groups in PVB via hydrogen bonding prompts a cohesive polymer network resulting in electrodes exhibiting superior rate capability and high ICE in both Li-ion and Na-ion laboratory-scale cells, surpassing the performance of those with other binders tested. After optimizing the formulations by using commercial PVB, we demonstrate for the first time the use of recycled PVB, sourced from laminated glass waste, to address the lack of end-of-life programs for this material, which often ends up in landfills. Repurposing PVB waste for battery applications tackles waste management issues and contributes to innovative development of advanced, green battery materials in a circular economy approach, thus paving the way for novel waste-to-energy solutions combining high-performance with socio-economical and environmental benefits.

1. Introduction

Lithium-ion batteries (LIBs) are widely employed in portable electronic devices and to power electric transportation in hybrid and electric vehicles. However, the finite and uneven distribution of lithium resources presents a significant challenge to the sustainable advancement of LIB technology.[1,2] Sodium-ion batteries (NIBs) are increasingly seen as a strong contender to LIBs in our future electrified society. Indeed, their potential for low costs, improved sustainability, and enhanced safety (at 0 V since their aluminum remains stable, unlike LIBs copper current collector),[3] while accounting for similar energy/power density, makes them highly suitable for residential, industrial, and remote location storage, as well as backup power systems, and affordable light electric vehicles.[4–6]

So far, extensive research has focused on anode materials for alkali metal-ion batteries, with carbonaceous materials drawing notable attention. This is due to their distinctive blend of properties, including good electronic conductivity, high practical capacity, relatively large surface area and limited volume change, excellent corrosion resistance along with high availability and cost-effectiveness.[7,8] Among them, amorphous carbon and graphite are frequently utilized. Carbonaceous materials are categorized into soft carbon orhard carbon (HC) based on whether it undergoes high- or low-temperature graphitization.[9]

HC was initially used as the anode material in Sony's second-generation LIBs. However, in the 1990s, graphite replaced HC in third-generation LIBs due to its superior initial Coulombic efficiency (ICE) and higher energy density.[10] Despite over 30 years of advancements, the performance of graphite-based LIBs has now reached a plateau, constrained by the limitations of current anode materials. As a result, HC is regaining attention for LIBs for its improved cycling ability, enhanced safety, and stability under low-temperature conditions.[11] HC, first introduced by David Stevens and Jeff Dahn,[12] is considered a promising anode material for NIBs as well due to its well-rounded performance characteristics. It features a moderate specific

H. Darjazi, A. Piovano, G. Meligrana, G. A. Elia, C. Gerbaldi
GAME Lab
Department of Applied Science and Technology
Politecnico di Torino
Corso Duca degli Abruzzi 24, Torino 10129, Italy
E-mail: hamideh.darjazi@polito.it; claudio.gerbaldi@polito.it
H. Darjazi, A. Piovano, G. Meligrana, G. A. Elia, C. Gerbaldi
National Reference Center for Electrochemical Energy Storage (GISEL) – INSTM
Via G. Giusti 9, Firenze 50121, Italy

The ORCID identification number(s) for the author(s) of this article can be found under https://doi.org/10.1002/adfm.202426075

DOI: 10.1002/adfm.202426075

capacity, a low operating potential of ≈0.2 V, cost-effectiveness, and a long cycle life. These advantages are attributed to its large interlayer spacing and complex internal structure, including various hindrances to ion diffusion and defects.[13,14] Despite its potential, HC encounters issues, such as low ICE and inadequate rate capability, obstructing its commercialization path.[15,16]

While most research to date has been directed toward adjusting the microstructure of HC anodes and finding compatible electrolytes, there is a shortage of studies on binders that are appropriate for HC anodes.[17] This oversight occurs because binders make up only a small fraction of the electrode composition and cell, and thus are often underestimated in terms of their impact on the overall cost of the final battery cells.[18,19] Nonetheless, binders play a crucial role, with their primary functions being to connect active material particles, ensure paste adhesion to the current collector, and withstand electrode volume changes during cycling. They must also be thermally and (electro)chemically stable and environmentally friendly.[20]

Poly(vinylidene difluoride) (PVDF) binder is commonly used in commercial battery cathodes due to its high chemical resistance and electrochemical stability in both LIBs and NIBs. Additionally, PVDF absorbs liquid electrolytes, facilitating transport of Li/Na to the active material surface.[21] However, it requires using N-methyl-2-pyrrolidone (NMP) as a solvent, which leads to high cost, toxicity, and flammability issues, thus necessitating strict protocols during all the phases of electrodes preparation, and following disposal and/or recycling. Additionally, the slower evaporation of NMP in organic-based slurries causes poorer PVDF uniformity compared to water-based electrodes. Furthermore, PVDF tends to migrate to the surface during the slow evaporation of NMP, potentially impacting adhesion, mechanical resistance, and CE.[22] Carboxymethyl cellulose (CMC) and polyacrylic acid (PAA) are widely used green binders that contain polar functional groups (—COOH, —OH, —O—). These groups enable strong interactions with active materials through hydrogen bonding, ion-dipole interactions, and chemical bonding, thereby enhancing the overall stability and performance of the electrodes.[23] Although CMC binders have good adhesion properties, they often face challenges, such as detachment from the active material upon cycling, which in turn leads to cracks, fracturation and pulverization of the electrode material.[24] To improve adhesion and mechanical stability, especially for high-thickness laminates, SBR (styrene-butadiene rubber) is often used in combination with CMC. The elastic nature of SBR helps enhance the overall durability and performance of the laminate during cycling.[25]

PAA as a binder offers several benefits, such as suitable mechanical properties and minimal swelling in electrolyte solvents.[26] Its chemical structure, with carboxylic acid moieties, allows for strong hydrogen bonds with active materials and substrates, especially through interactions with polar groups at the edges of carbon planes. Studies by Fan et al.[27] and Chen et al.[28] showed that using a PAA binder improves performance and increases ICE for nitrogen-doped hollow carbon nanotubes and FeS, respectively. This enhancement is attributed to the electrochemical activity of PAA, reduced internal resistance in the electrode, and the formation of a uniform passivation layer that stabilizes the electrode. However, the highly polar nature of PAA leads to weak adhesion to the current collector, causing it to delaminate easily from the substrate, particularly when mass loading is increased.[29]

Considering that one of the main ambitions of NIB technology is to be a sustainable alternative to LIBs, the focus on utilizing recycled materials is particularly relevant given that the traditional linear production model, where products move from the cradle to the grave —from production to consumption to waste — has contributed to the mismanagement of environmental resources, especially as the global population grows.[30] In response to this challenge, the concept of a circular economy is gaining attention, where waste and surplus materials are transformed into secondary raw materials. This shift not only helps conserve energy but also plays a crucial role in environmental protection by converting waste into valuable resources. The use of recycled and waste materials is increasingly recognized as a key approach in various industries, including battery manufacturing, to make production processes greener and more sustainable. However, significant challenges remain, such as securing widespread manufacturer adoption of recycled materials over virgin raw materials. Overcoming these barriers will require investments in scaling up recycling technologies, utilizing high-quality data, and creating stable demand for sustainable products. Ultimately, this industry transformation is driven by the growing consumer demand for environmentally friendly goods, making waste utilization a pivotal factor in the future of sustainable production, thus benefiting the economy, environment and society.

In such a scenario, this study introduces for the first time the use of recycled polyvinyl butyral (PVB) as a binder for HC in both LIBs and NIBs. PVB is highly regarded for its strong adhesive properties, resilience, and flexibility,[31] making it a common choice in various industrial applications, such as in laminated safety glass; such advantageous properties at a macroscopic level are originated at a molecular level by the presence of many different functional groups and a complex dynamic of the polymer chains and pendant groups.[32] Currently, most post-consumer PVB from laminated glass is either incinerated or landfilled, with only 9% being recycled. The SUNRISE European project (https://sunrise-project.eu/) aims at developing an efficient pathway for post-consumer PVB (up to 125000 tons per year expected), automatically separating it into a high-quality fraction to be reused for its original purpose in laminated glasses, and a low-quality fraction to be repurposed in valuable secondary applications such as energy storage devices, either as membrane for electrolyte separator[33] or as binder in electrodes preparation. The non-polar butyral groups in PVB enhance its adhesion to conductive carbon additives and improve electrolyte absorption, which boosts Li^+/Na^+ ions conductivity. However, the significant presence of acetal (butyral) groups could cause the polymer to soften in electrolytes, potentially weakening its mechanical stability.[34] The study investigates blends of PVB with PAA and PVDF, aiming to create dual-binder systems that harness these materials combined strengths and mitigate the issue associated with the mechanical stability of using only PVB. The obtained results are compared with the performances of analogues electrodes prepared with only PVDF or PAA as binder and tested in the same conditions, in order to clearly point out the effect of PVB addition in the binder formulation. Our study not only demonstrates the potential use of PVB in the battery field but, noteworthy, first shows that recycled PVB (commercial

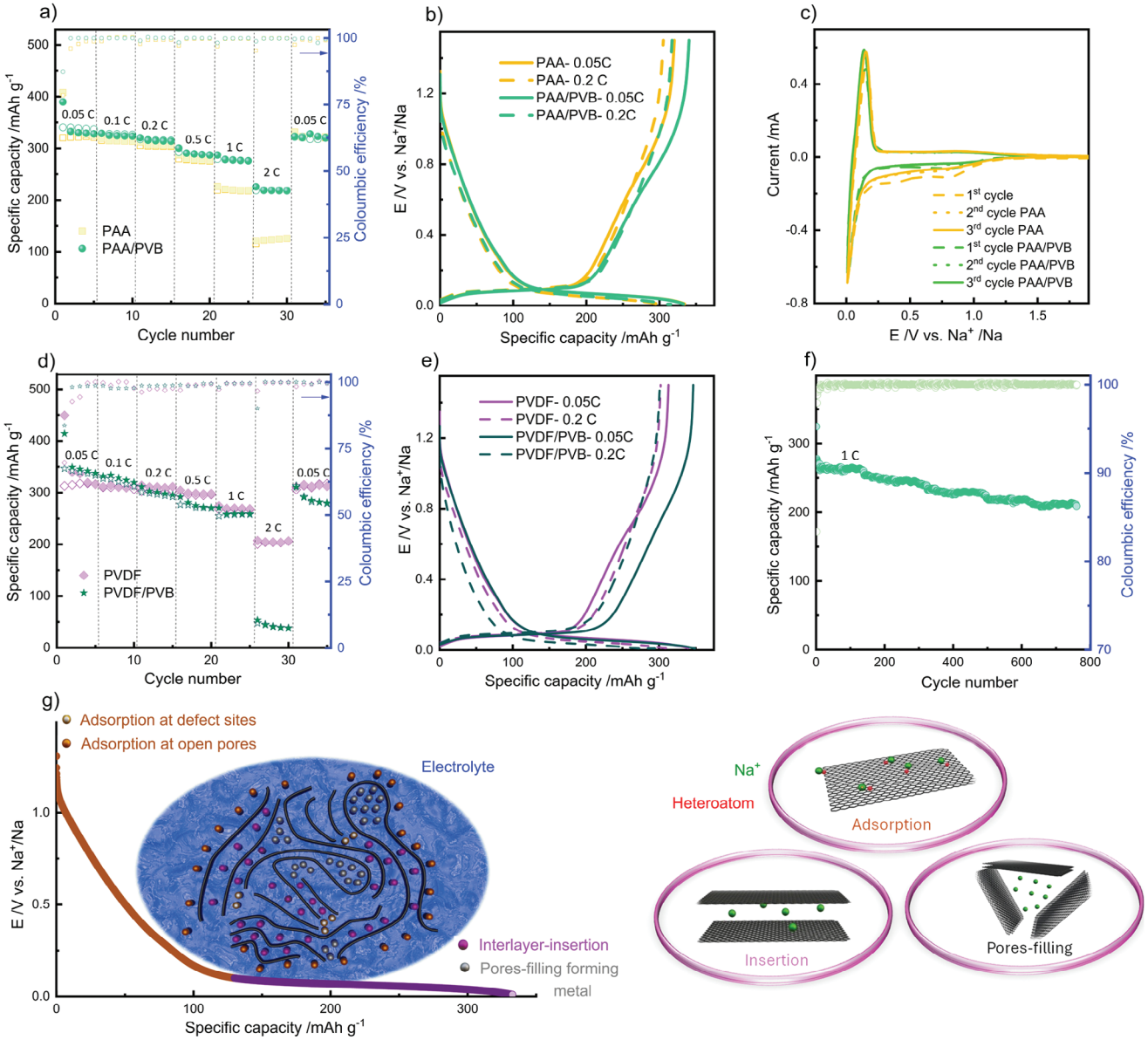

Figure 1. Rate capability and galvanostatic discharge/charge voltage profiles for NIB electrodes based on PAA and PAA/PVB binders a,b); CV curves acquired during the first three cycles, scan rate 0.05 mV s^{-1} for electrodes based on PAA and PAA/PVB binders c); rate capability and galvanostatic discharge/charge voltage profiles for electrodes based on PVDF and PVDF/PVB d,e); cycling performances of PAA/PVB-based electrode at 1 C f); the current theoretical models for Na-storage g).

one is used for initial validation/testing), sourced by the SUNRISE European project from automotive laminated glass waste, can be straightforwardly implemented as electrode component in LIB/NIB devices.

2. Results and Discussion

2.1. Na Storage Performance

To assess the electrochemical response of electrodes prepared with PAA, PAA/PVB (80/20), PVDF, and PVDF/PVB (80/20) binders across various current densities, and to analyze the influence of these binders on the charge/discharge characteristics, all electrodes underwent testing to determine their C-rate capabilities. Charge and discharge cycles were conducted ranging from 0.05 C to 2 C and back to 0.05 C within the voltage window of 0.01–1.5 V versus Na^+/Na (**Figure** 1a,d). During the initial cycle at 0.05 C, electrodes based on PAA, PAA/PVB, PVDF, and PVDF/PVB display discharge capacities ranging from 389 to 449 mAh g^{-1}, with corresponding CE of ≈78.5%, 87.3%, 69.9%, and 83.7%, respectively. The irreversible capacity observed in the initial cycle can be ascribed to the extensive specific surface area of the HC material, leading to significant electrolyte decomposition at the carbon surface and subsequent SEI layer formation.[36] In

the second cycle at 0.05 C, the PAA/PVB-based electrode exhibits a reversible discharge capacity of 332.7 mAh g^{-1} with a high CE of 99.9%, and it maintains almost the same reversible capacity up to 0.2 C. Most notably, the capacity only slightly decreases at 1 C at 278.5 mAh g^{-1} and even at 2 C the capacity is still as high as 225.7 mAh g^{-1} (always accompanied by a high CE of 99.9%). The latter values at high currents surpass those of electrodes based on PAA, PVDF, and PVDF/PVB tested in the same conditions. The superior rate performance of the PAA/PVB-based electrode can be attributed to the chemical structure of the PVB polymer, which presents potential advantages for application in HC anodes. Indeed, the ability of the COOH groups of PAA and the OH groups of PVB to form hydrogen bonds results in the formation of a polymer network in PAA/PVB mixtures when used as two-component binders. This network combines the advantageous properties of both polymers. In addition, PVB contains non-polar butyral groups (alongside the polar hydroxyl groups already discussed), which confer to the prepared electrodes a significantly improved adhesion to conductive carbon additives and an enhanced uptake of the organic solvent-based electrolyte. Overall, these aspects lead to improved Na^+ ion conductivity in the electrode system.[37]

Furthermore, the increased ICE observed in the PAA/PVB-based electrode, comparable with the ICE of graphite electrodes in Li half-cells (≈90%), may be attributed to its improved coverage of the HC particles and in particular to the hydrogen bonds formed by PVB with the oxygen-rich functional groups typically present at the edges of HC graphitic domains thus limiting their exposition and reactivity. This enhanced coverage potentially minimises the excessive consumption of the electrolyte, thereby augmenting the CE in the first cycles and during subsequent cycles.[23]

The storage of sodium in HC materials continues to be a topic of ongoing discussion, largely due to the complexity inherent in the microstructure of HC. This complexity encompasses various factors such as heteroatoms, defects, edge sites, lateral size, thickness of graphitic layers, and micropores.[38] Furthermore, this issue arises from the constraints of current characterization techniques. Thus, a thorough examination of the galvanostatic charge/discharge curves was conducted to gain a comprehensive insight into Na insertion within the HCs. Figure 1b,e illustrates the voltage profiles of all electrodes at rates of 0.05 C and 0.2 C, respectively. These curves exhibit two prominent regions: a high voltage range spanning from 1.5 to 0.1 V, identified as the sloping region, and a low potential area below 0.1 V, known as the plateau region. The storage of sodium in both the high-voltage sloping region and low-voltage plateau region can be categorized based on existing models. These categories include the "insertion-adsorption" model, the "adsorption-insertion" model, the "adsorption-insertion-nanopore filling" multistage (three-stage) model, and the adsorption-nanopore filling" model.[39] The adsorption of Na^+ in the slope region and the intercalation of Na^+ in the plateau region have been validated through various characterisations. Additionally, the pore filling of HC in the plateau region has been progressively confirmed, providing a consistent explanation for a wide range of experimental results. Therefore, we believe that the "three-stage' model, illustrated in Figure 1g, is the most convincing mechanism among the proposed theories.[40,41] This suggests that the high-potential sloping curve is attributed to the adsorption of alkali ions at defect and edge sites as well as in open pores, while the low-potential plateau corresponds to intercalation between parallel graphene sheets and the pore-filling process.

The Na storage behavior of both PAA- and PAA/PVB-based HC is further elucidated by the CV curves shown in Figure 1c. Notably, the pore-filling and specific intercalation peaks are observed near 0.01 V, while a weaker peak ≈1.0 V is attributed to the adsorption of sodium ions at heteroatoms, edges, and other defects within the carbonaceous materials.[42,43] Noteworthy, the initial irreversible peak during the first cathodic scan is less prominent for the PAA/PVB-based electrode compared to the PAA-based one. This observation aligns well with the higher ICE of the PAA/PVB-based electrode. Furthermore, in Figure 1f, the long-term cycling performance at 1 C of the PAA/PVB-based electrode is provided to assess its cycling stability. Remarkably, even after more than 750 cycles, the electrode retained a capacity of 213 mAh g^{-1}, corresponding to a capacity retention of 77% (versus initial capacity) and CE of 99.9%. Kindly note that the cell was tested at ambient laboratory temperature (up to 5 °C fluctuations) and not thermally equilibrated at a fixed temperature.

EIS was conducted every ten cycles to elucidate the interfacial behavior of electrodes with different binders and, more specifically, the effect of PVB as a binder. **Figure 2**a,b shows the Nyquist plots recorded using PAA and PAA/PVB binders, respectively. All impedance spectra exhibit similar characteristics (see the insets of Figure 2a,b): i) a semicircle at high frequencies corresponding to migration through the passivation layer, partially overlapped by ii) a semicircle at mid frequencies associated with the interfacial charge-transfer process; iii) a sloped line at low frequencies linked to Na^+ ion diffusion in the bulk of the active materials.[44,45] EIS data were fitted using the following equivalent circuit model noted as $R_{sol}(R_{SEI}\ C_{SEI})(R_{CT}C_{DL})WC_i$ in the notation of Boukamp. The model includes R_{sol}, representing the Na-ion resistance across the electrolyte solution; R_{SEI} and C_{SEI}, indicating the resistance and capacitance of the solid electrolyte interphase; R_{CT} and C_{DL}, denoting the charge-transfer resistance and double-layer capacitance; Warburg diffusion (W), related to the solid-state diffusion of Na-ions; and C_i, representing differential intercalation. Due to the roughness of the electrodes, all capacitance elements (C) were replaced by constant-phase elements (Q). The evolution upon cycling of calculated values of R_{sol}, $R_{SEI,}$ and R_{CT} is shown in Figure 2c. The R_{sol} values for both samples remain constant during cycling; however, the PAA/PVB-based sample exhibits lower resistance values, suggesting that the electrolyte decomposes to a lesser extent. It clearly explains the better ICE of PAA/PVB-based anode. In terms of passivation layer resistance, the R_{SEI} values for both anodes increase with cycling. Nevertheless, the PAA/PVB-based electrode demonstrates more stable behavior after 80 cycles. Regarding R_{CT} values, both electrodes demonstrate stable behavior. However, the PAA/PVB anode shows lower values than the PAA-based electrode, indicating improved kinetics and overall performance.

GITT is a robust method that connects charge kinetics with thermodynamics in insertion compounds, and it is suitable for evaluating diffusion behavior. Therefore, GITT was conducted on PAA and PAA/PVB-based anodes, and the apparent diffusion coefficients were calculated, as illustrated in Figure 2d,e. During sodiation, the diffusion coefficient (D_{Na+}) steadily declines

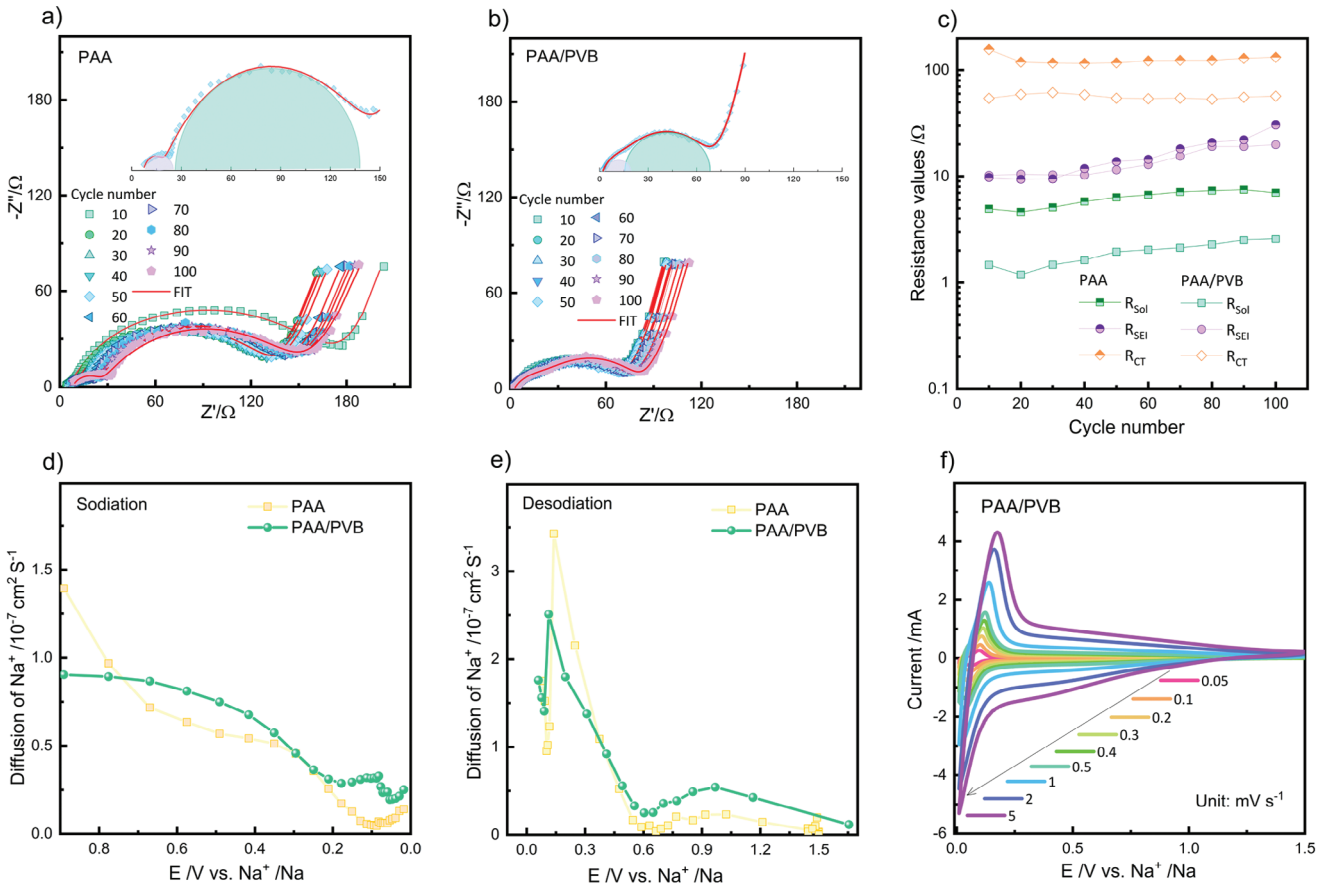

Figure 2. Nyquist plots of NIB electrodes prepared with PAA a) and PAA/PVB b) binders: resistance values upon cycling, as calculated by EIS data analysis c); Na^+ apparent diffusion coefficients acquired from GITT for NIB electrode prepared with PAA and PAA/PVB binders during sodiation d) or desodiation e); CV profiles of PAA/PVB based electrode acquired at different scan rates f).

until the voltage for Na^+ reached 0.1 V in the PAA-based electrode and 0.05 V in the PAA/PVB-based electrode, despite some fluctuations observed. Upon reaching the cut-off voltage in both electrodes, there is an increase in the D_{Na+} value for Na^+, with a notably higher value observed for the PAA/PVB-based electrode (Figure 2e). During the desodiation process, the diffusion coefficient initially decreases, followed by an increase; subsequently, it decreases again before reaching the cut-off voltage (Figure 2d). The initial high D_{Na+} values during sodiation, aligning with the sloping voltage region, are ascribed to the adsorption of Na^+ ions at HC surface active sites (e.g., edges, defects, and micropore surfaces), facilitated by the ready access of Na^+ ions. It follows that the repulsive forces induced by the preadsorbed Na^+ ions at high voltage lead to a decrease in the D_{Na+} value.[38] As these surface sites gradually fill up, Na^+ ions begin inserting into the graphitic layers and pore filling, marking the onset of the plateau region. This increase is especially advantageous for fast charging. If the diffusion rate of Na^+ ions is lower than the migration rate, metallic sodium may deposit on the electrode surface. Consequently, achieving a high sodium ion diffusion rate at the end of sodiation can help minimise the risk of such plating.[39,46] At the beginning of sodiation, the PAA-based electrode exhibits a higher D_{Na+} value, likely due to its more defective structure, which enhances the sodium ion diffusion rate for adsorption. However, as sodiation progresses, the PAA/PVB-based electrode demonstrates higher values, indicating that this blend facilitates a faster process for sodium ions to pass through the pores and insert between layers.

To delve deeper into the ion carrier storage mechanism, CV was carried out across a range of scan rates from 0.05 to 5 mV s^{-1} (see Figure 2f). The insertion of ions into layers typically follows a diffusion-controlled insertion/deinsertion process while the adsorption of ions at defects (such as edges), surfaces, or functional groups, is characterized by surface-driven pseudocapacitive reactions. As shown in Figure 2f, as the scan rate increased, a slight shift in the oxidation peak toward higher potentials was observed, showing the onset of slow polarisation of the material. The power-law relationship between scanning rate (ϑ) and peak currents (i) was calculated by fitting the data using the equation $i = a\vartheta^b$ (where a and b are both adjustable constants),[47] shown in Figure S1 (Supporting Information). Specifically, a value of $b = 0.5$ signifies diffusion-controlled reactions, while $b = 1$ represents surface-controlled reactions. Two peaks were selected for the kinetic analysis: the first is a broad peak at 0.7 V (denoted as i_b), corresponding to the sloping region, and the second is a sharp peak at a lower potential of 0.01 V (denoted as i_a). The relationship between the current peaks and scan rate, plotted on a logarithmic scale, is shown in Figure S1a,b (Supporting Information). Both

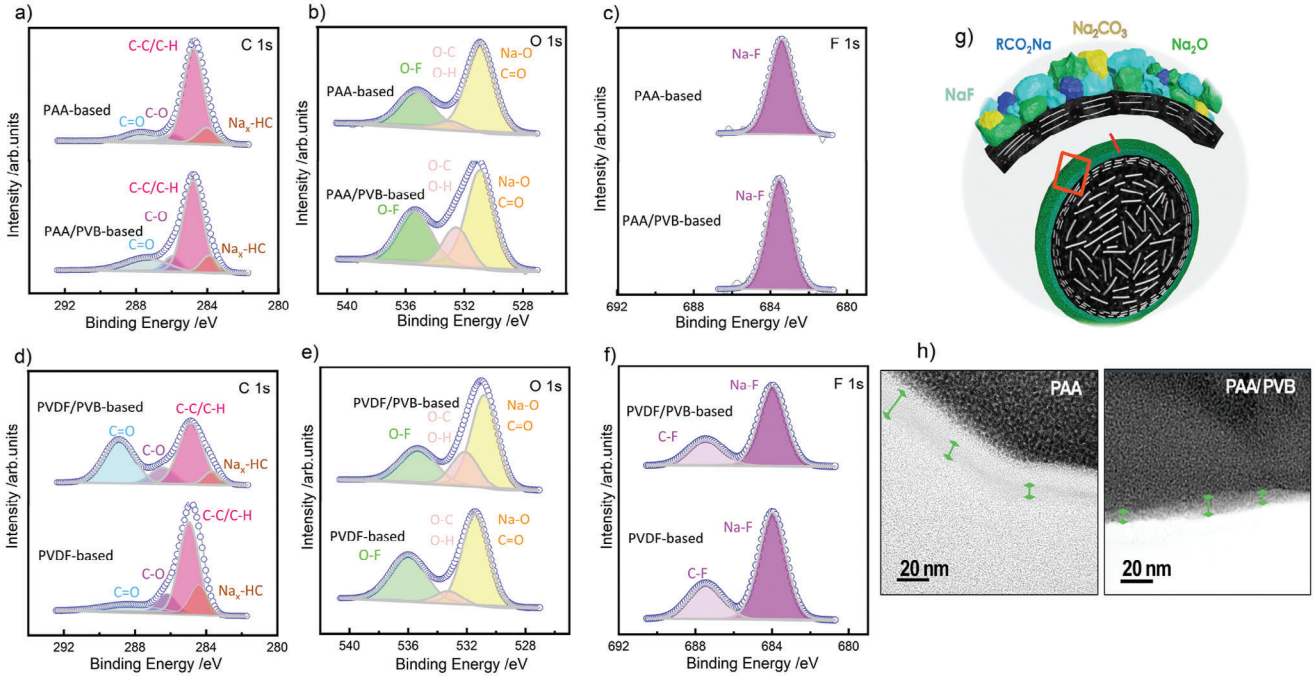

Figure 3. XPS spectra of C 1s a,d), O 1s b,e), and F 1s c,f) of cycled HC electrodes based on different binders; SEI formation and proposed composition g); HRTEM images of cycled HC electrodes h).

curves exhibit an excellent linear fit with $R^2 = 0.98 - 0.99$. The calculated *b* value for the sharp peak is 0.61, which points to a diffusion-controlled process at lower potentials. In contrast, the *b* value for the broader hump is 0.86, indicating a non-diffusion mechanism, such as surface-driven or pseudocapacitive behavior for the sodium storage in this potential range.[48]

2.2. NIB Electrode Interface and Morphological Characterization

The SEI layer on the HC anode significantly influences the battery performance by impacting both impedance and the diffusion ability of Na^+ ions. **Figure 3** provides insights into the specific chemical components within the SEI layer obtained through XPS analysis to better understand the impact of PVB as a copolymer binder. The analysis unveils the composition of the SEI layer formed during the cycling of HC electrodes. The evaluation focuses on analysing C1s, O1s, and F1s peaks in cycled HC electrodes prepared with PAA, PAA/PVB (80/20), PVDF, and PVDF/PVB (80/20) binders. Table S1 (Supporting Information) details the precise XPS fitting peaks and their corresponding binding energies. In Figure 3a,d, distinct carbon fingerprints reflect the various carbon-based species in the SEI. These include binding energy at 283.9–283.8 eV, which account for C associated with the sodiated Na_x-HC electrode; 284.7–284.8 eV, suggesting the presence of C atoms bound exclusively to H or other C atoms (C-C/C-H), generally associated with aliphatic chains, including the fraction of polymer binder,[49,50] mixed degradation byproducts common hydrocarbon contaminations; 285.9 eV, indicating C atoms bound to single oxygen (C-O); and 287.7–287.4 eV, associated with C═O moieties.[51] Such COO moieties are likely associated with species originating from the degradation of electrolyte solvents (EC and DMC). This process involves breaking one C—O bond of the carbonate group, forming species like R—COONa.[52] The electrode based on PVDF/PVB (80/20) exhibits the highest intensity of C—O and C═O components, whereas the PAA/PVB (80/20)-based electrode remains almost similar to PAA- and PVDF-based electrodes. This suggests that Na_2CO_3 and R—COONa are more prevalent on the surface of the PVDF/PVB (80/20)-based electrode. The peaks corresponding to C-H, C-C also indicate organic species generated through the reduction of solvents within the SEI. Aliphatic chains (C—C/C—H components) are found in the SEI for all electrodes;[53] however, the quantity of these chains decreases for the PVDF/PVB (80/20)-based electrode after cycling. Indeed, compared to other electrodes, the PVDF/PVB (80/20)-based electrode exhibits a significantly weaker intensity of the Na_x—HC signal in the C1s peaks. This attenuation is attributed to the thick SEI layer formed on the HC, which obstructs the Na_x—HC signal.[54] In contrast, PVDF- and PAA/PVB (80/20)-based electrodes show a slightly higher Nax—HC signal intensity.

In Figure 3b,e, the O1s peak observed at ≈533 eV (attributed to O—H and O—C) is linked to the presence of organic species resulting from the reduction of solvents within the SEI formation. The PVB-based electrodes exhibit a slightly higher intensity of this component compared to other electrodes, which is reasonable considering that PVB itself is rich in O-H and O—C moieties.[55] The O1s peaks detected at ≈531 and 536 eV are associated with inorganic compounds containing Na—O and Na—O—F, respectively. Notably, these inorganic compounds do not involve reductions associated with solvent complexes.[54] The high intensities of these peaks in the PAA/PVB (80/20)-based electrode suggest a heightened concentration of organic and inorganic species within the SEI.

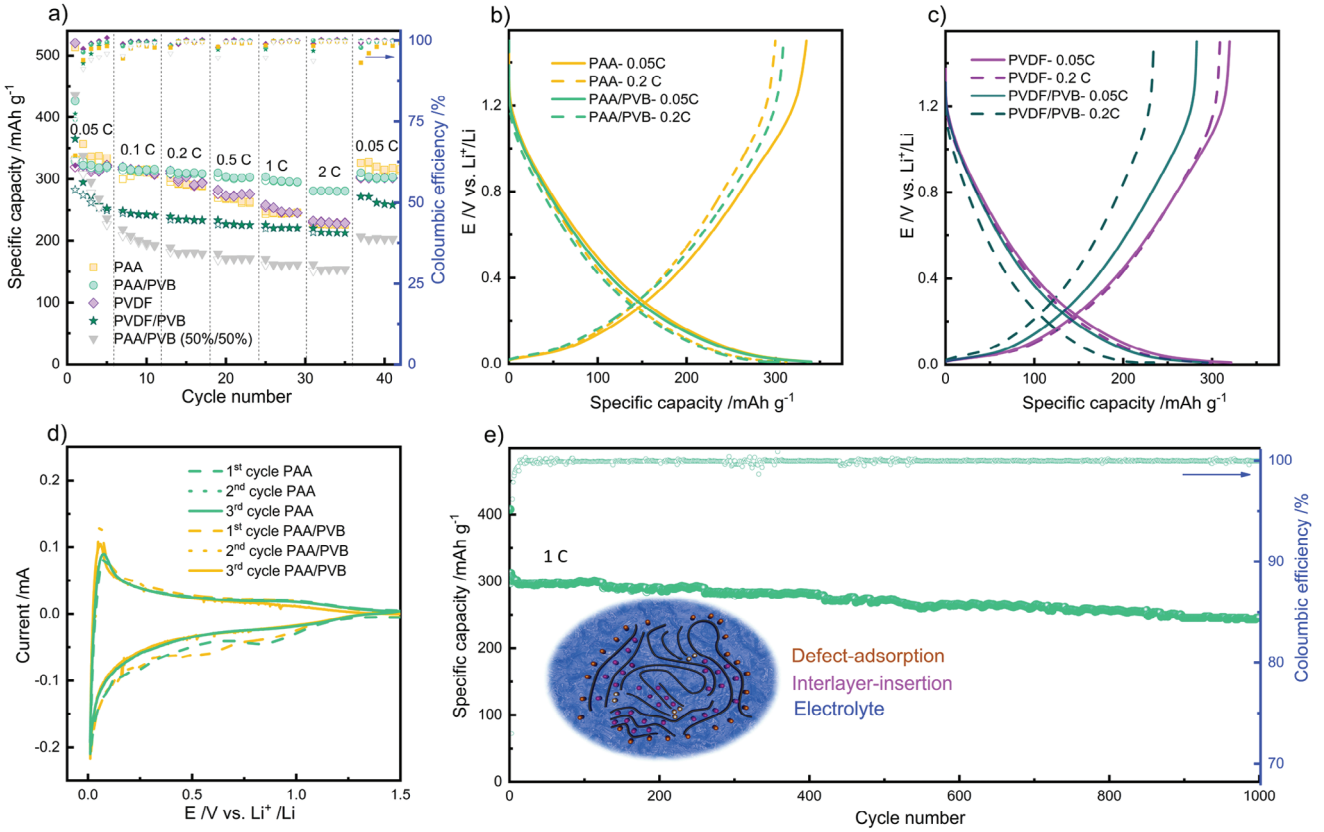

Figure 4. Rate capability and galvanostatic discharge/charge voltage profiles for LIB electrodes based on PAA, PAA/PVB, PVDF, and PVDF/PVB binders a); galvanostatic discharge/charge voltage profiles for electrodes based on b,c); CV curves acquired during the first three cycles, scan rate 0.05 mV s^{-1} for electrodes based on PAA and PAA/PVB d); cycling performances of PAA/PVB/based electrode at 1 C e).

The F1s XPS peaks (Figure 3c,f) exhibit a distinct signal at 683.5 eV (attributed to Na-F) across all electrodes. Additionally, a peak at 687.5 eV was observed exclusively in PVDF-based electrodes.[53] This peak may originate from the C-F bond of PVDF.[56] When comparing electrodes utilizing different binders, electrodes based on PAA/PVB (80/20) exhibit a higher concentration of NaF, which can play an important role in stabilizing the SEI and allowing for a more efficient ion transfer.

Figure 3h displays HRTEM images of HC electrodes using PAA and PAA/PVB (80/20) after 10 cycles, offering a clearer understanding of how PVB influences PAA to improve electrode performance. Indeed, the SEI layer on the HC electrode with PAA/PVB (80/20) is dense and uniform, consistent with XPS results. However, the SEI layer exhibits uneven thickness in the HC-PAA electrode and lacks uniformity.

SEM analysis was carried out on electrodes made with various binders—PAA, PAA/PVB (80/20), PVDF, and PVDF/PVB (80/20)—both before and after cycling to assess the impact of these binders on the morphology and particle aggregation of the electrodes. Figure S2 (Supporting Information) illustrate the surface morphology of the electrodes prepared for NIBs. It is evident that electrodes utilizing PAA and PAA/PVB (80/20) binders (panels a, b, e, f) demonstrate a more uniform particle distribution and reduced aggregation compared to those with PVDF and PVDF/PVB (80/20) binders (panels c, d, g, h), both before and after cycling. Notably, the PVDF/PVB (80/20) electrodes exhibit substantial particle agglomeration (panel d) and the formation of intergranular microcracks upon cycling (panel h). These cracks are believed to impair contact among the particles and between the active material particles and the current collector. Moreover, the formation of these cracks may increase the interfacial area exposed to side reactions, leading to excess/thicker SEI formation, as evidenced by XPS, thus in turn gradual loss of active material, which could explain the observed capacity loss during the initial cycles.

2.3. Li Storage Performance

The electrochemical performance of electrodes based on different binders was confirmed in laboratory-scale Li-metal cells, by carrying out galvanostatic cycling and CV, as shown in **Figure 4**. In this study, we also attempted to increase the amount of PVB to 50% in the electrode composition (namely, PAA and PVB in a 50/50 mass ratio) and resulting electrode performance was tested. Figure 4a shows the rate capability test of all electrodes within the voltage window of 0.01 to 1.5 V versus Li^+/Li. Electrodes based on PAA, PAA/PVB (80/20), PAA/PVB (50/50), PVDF, and PVDF/PVB (80/20) display discharge capacities ranging from 365 to 520 mAh g^{-1} at 0.05 C, in the first cycle, with corresponding CE of ≈64.5%, 75.6%, 75.5%, 61.4%, and 77.4%, respectively. As mentioned before, the irreversible capacity in the

first cycle can be associated with the electrolyte decomposition and subsequent SEI layer formation.[36] The enhancement of ICE with the addition of PVB is also evident in Li-based cells. This improvement is likely due to the PVB ability to provide better coverage over the HC particles, thereby covering surface imperfections and reducing side reactions. In the 2nd cycle at 0.05 C, the PAA/PVB-based (80/20) electrode exhibits a reversible discharge capacity of 322.5 $mAhg^{-1}$, whereas in the 30th cycle at 2 C the exhibited value is still as high as 280.6 $mAhg^{-1}$, accompanied by a high CE of 99.97%. These values exceed those of electrodes based on PAA, PVDF, and PVDF/PVB at high C-rates. Regarding PAA/PVB (50/50)-based electrode, the cell exhibits capacity loss at 0.05 C during the initial cycles, likely due to the electrode softening in the electrolyte upon cycling,[37] resulting in the loss of active materials. As a result, the PAA/PVB (80/20)-based electrode is confirmed to exhibit superior rate performance also in Li-metal cell configuration, surpassing even the performance observed in the Na half-cell. This enhanced performance can be attributed to the optimized binder composition, which effectively integrates the strengths of both components.

Figure 4b,c shows the voltage versus specific capacity profiles of electrodes using different binders at rates of 0.05 C and 0.2 C, which are typical of HC for LIBs.[57] Similar to NIBs, the mechanism of Li-ion insertion in HC remains a topic of ongoing debate. However, based on the analysis of numerous research findings, there is growing support for the "adsorption-intercalation" mechanism.[58] It is important to note that Li^+ ions can intercalate into graphitic layers more easily than Na^+ ions, forming a stable lithium-graphite intercalation compound (Li-GIC), such as LiC_6. The less favorable intercalation of Na^+ ions is primarily due to their larger ionic radius and the thermodynamic instability of the Na-rich GICs (NaC_6 and NaC_8). Yang and colleagues used ^{7}Li NMR to investigate lithium in porous carbon discharged to 0.0 V and lower.[48] They observed ^{7}Li signals near 0 ppm from carbon-lithium compounds as well as lithium ions, suggesting that both intercalation between graphite layers and adsorption were taking place. However, no signal shift indicating lithium filling the pores was detected until the carbon was discharged below 0.0 V. These results led them to support an adsorption-intercalation mechanism.[48,59]

The CV curves for PAA- and PAA/PVB- based electrodes in Figure 4d reveal that the anodic peak shifts from 0.13 V for Na (Figure 1c) to ≈0.05 V for Li, highlighting the impact of ionic size. Additionally, a distinct anodic peak ≈1.0 V versus Li^+/Li for Li, which is hardly detectable for Na, suggests that chemical binding interactions weaken as the alkali metal ions increase in size.[57] These observations are consistent with the voltage profile data.

Figure 4e highlights the long-term cycling performance of the PAA/PVB-based electrode, tested to assess its stability over time. The electrode was subjected to galvanostatic charge/discharge cycling at a 1 C rate and delivered outstanding results, maintaining a capacity of 250 mA h g^{-1} even after 1000 cycles, corresponding to a capacity retention of 81.4% (versus cycle 10th), with a CE of 99.9%. The measurements were carried out at ambient temperature; the capacity fluctuations observed during the prolonged cycling are attributed to day/night temperature variations.

To clarify the interfacial behavior of PAA- and PAA/PVB-based electrodes, EIS was performed every ten cycles for LIBs as well (**Figure** 5a,b). EIS data were analyzed using the same equivalent circuit model employed for NIBs, with the calculated values of R_{sol}, R_{SEI}, and R_{CT} shown in Figure 5c. As observed, the R_{sol} values remain constant during cycling for both anodes. However, the PAA-based anode exhibits significantly higher values compared to the PAA/PVB-based anode, indicating reduced electrolyte decomposition in the latter, which explains its superior ICE. For the R_{SEI}, values for the PAA-based anode increase up to 40 cycles, whereas the PAA/PVB-based anode shows stable R_{SEI} values. In terms of R_{CT}, the PAA-based anode experiences an increase in R_{CT} with cycling, while the PAA/PVB-based anode maintains constant values, indicating enhanced kinetics and overall electrochemical performance.

The GITT was used to study the PAA- and PAA/PVB-based anodes in LIBs as well, with the apparent diffusion coefficient (D_{Li+}) calculated according to Fick's second law of diffusion, as described in section 3.1. The findings are shown in Figure 5d,e. During lithiation, the diffusion coefficients for both anodes gradually decrease until the cut-off voltage is reached (Figure 5d). This suggests that once Li^+ ions initially occupy high-energy sites, subsequent ions tend to occupy less energetically favourable sites, which prolongs the diffusion pathway. In contrast to the behavior observed in NIBs, where the diffusion coefficients increase again below 0.1 V, the D_{Li+} values for LIBs do not exhibit a similar rise (this is additional proof for the absence of the pores filling step in LIBs). During de-lithiation, the diffusion coefficient decreases with increasing voltage, indicating that as Li^+ ions are released from lower-energy sites at low voltages, the remaining ions desorb from higher-energy sites at elevated voltages. Notably, the difference between the two anodes becomes apparent at the end of the lithiation and de-lithiation processes, where the D_{Li+} is higher for the PAA/PVB-based anode, indicating enhanced diffusion kinetics. In the CV curves (Figure 5f), two distinct peaks are observed at ≈0.01 V (i_a) and 0.70 V versus Li^+/Li (i_b) during cathodic scans. The calculated *b* value (Figure S1c,d, Supporting Information) for the sharp peak is 0.56, suggesting a diffusion-controlled process at lower potentials. On the other hand, the *b* value for the broader hump is 0.78, indicating that lithium storage in this potential range is primarily dominated by a surface-controlled or non-diffusion mechanism. This difference highlights the varying lithium-ion storage mechanisms at different voltage regions.[60]

2.4. Recycled PVB-Based Electrode

As we mentioned, the global PVB market is expected to experience significant growth in the coming years, driven by increasing industrialization and urbanization rates. Projections estimate that the market will reach approximately USD 3641.25 million by 2031.[61] However, despite this growth, end-of-life management for PVB remains inadequate, with large volumes of PVB film ending up in landfills. Recycling valuable PVB waste has thus become increasingly important within the context of circular and sustainable material practices, and the European "SUNRISE" project specifically addresses this need by focusing on the recycling of PVB, and reuse of the non-recyclable fraction in high-value-added applications like energy storage devices. Given the unique properties of PVB films and the limited research on applications involving recycled PVB (re-PVB), this study initially employed commercial PVB to determine the optimal

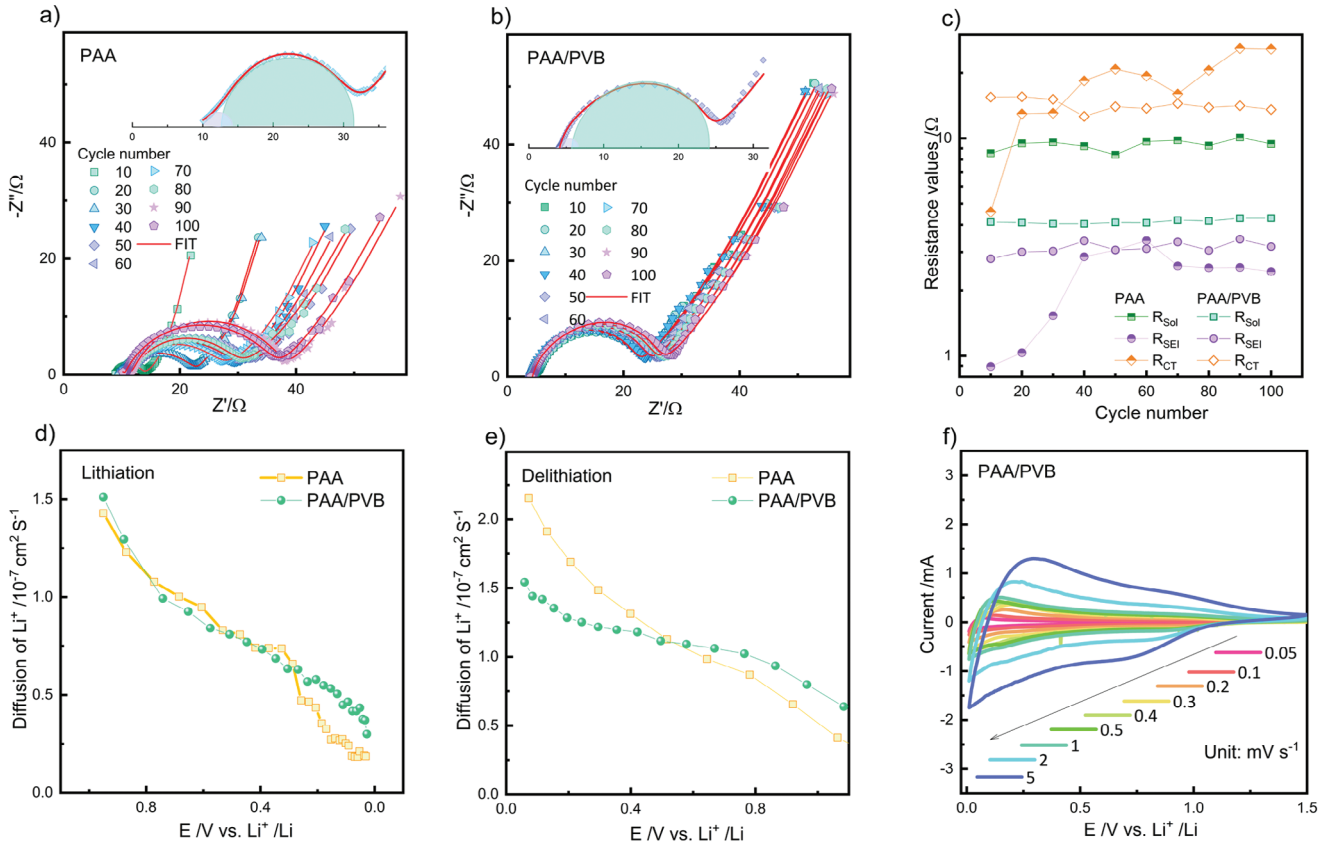

Figure 5. Nyquist plots of LIB electrodes prepared with PAA a) and PAA/PVB b) binders; resistance values upon cycling, as calculated by EIS data analysis c); Li^+ apparent diffusion coefficients acquired from GITT for LIB electrode prepared with PAA and PAA/PVB binder during lithiation d) and de-lithiation e); CV curves of PAA/PVB based electrode acquired at different scan rates f).

composition. Once identified, we proceeded to test a blend of PAA and re-PVB in a 80:20 mass ratio (**Figure 6**), with the re-PVB sourced from automotive glass waste through a patented mechanochemical process[62] Previous studies have analyzed this particular re-PVB using FT-IR, TGA, and NMR, demonstrating that the mechanochemical recycling process does not affect the molecular weight of the polymer (ca. 135000 g mol^{-1}, with a broad distribution), and identifying the presence of various plasticisers, all from the diester class, with an estimated polymer-to-plasticiser weight ratio of ≈1:1.[55] All the experimental procedures were performed following the same approach as with commercial PVB.

As clearly shown in Figure 6a, the laminates made from flake-shaped re-PVB exhibit excellent flexibility and strong mechanical properties with no particle detachment. These laminates adhere well to copper and aluminum current collector foils, ensuring good structural integrity.

The lithium and sodium storage performance of the PAA/rePVB electrode was characterized by galvanostatic discharge/charge and CV (Figure 6b–e). When tested as anodes, the electrodes with the PAA/rePVB binder exhibited reversible discharge capacities of 294.7 and 319.0 $mAhg^{-1}$ at 0.05 C laboratory-scale LIB and NIB cells, respectively. Even at 2 C, they retained capacities of 213.2 (LIB) and 211.2 $mAhg^{-1}$ (NIB), highlighting their strong rate performance across both technologies (Figure 6b). Additionally, the CE of both electrodes is relatively low at lower C-rates, which is ascribed to the presence of plasticisers and impurities in the recycled PVB undergoing degradation upon the first discharge/recharge cycles. Noteworthy, the CE improves significantly at higher C-rates.

Figure 6c,d shows the voltage versus specific capacity profiles of electrodes in both Li-ion and Na-ion laboratory-scale battery cells at rates of 0.05 C and 0.2 C, which are comparable to those observed with commercial PVB. Notably, the two cells exhibit different behaviors in the plateau regions for LIBs and NIBs, likely due to pore filling in the HC, which is confirmed in the case of NIBs. CV was performed for both systems to investigate the reaction mechanisms further during reversible lithium and sodium storage (Figure 6e). The resulting voltammograms closely resemble those obtained with commercial PVB, indicating that the side reactions of plasticisers are almost negligible and no additional redox processes and/or significant side reactions are introduced by the recycled PVB binder. Thus, re-PVB proves to be an effective binder for carbon-based energy storage materials in both LIBs and NIBs, aligning with sustainable development goals. This efficient strategy enhances both sodium and lithium storage performance, presenting a promising pathway for the development of low-cost, sustainable advanced anode materials by circular economy approach.

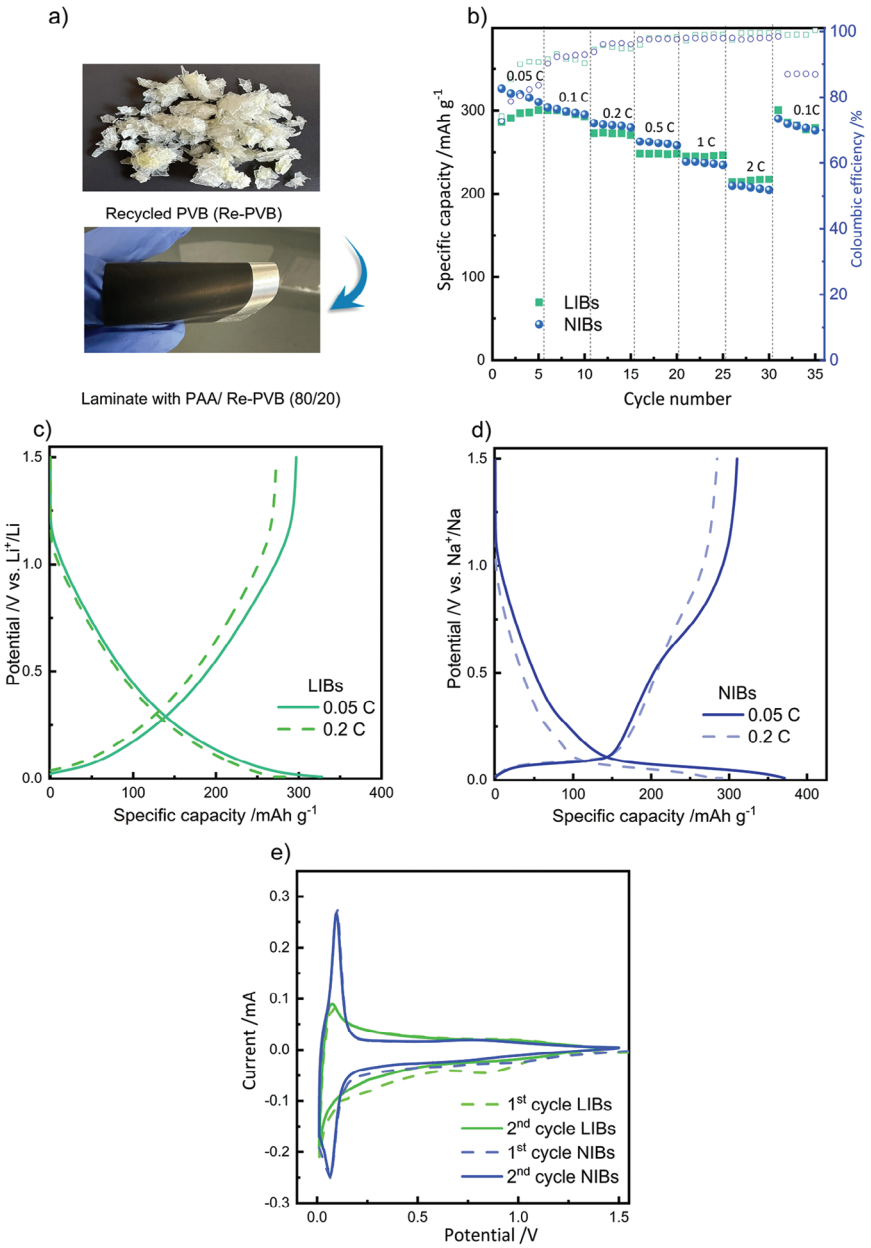

Figure 6. Digital photograph of the re-PVB and laminate with PAA/re-PVB a), rate capability b), galvanostatic discharge/charge voltage profiles c,d) and CV e) for LIB and NIB electrodes based on PAA/re-PVB.

3. Conclusion

The growing demand for high-performance renewable energy technologies, paired with socio-economic and environmental concerns, underscores the need for innovative, sustainable energy storage solutions. Under the accelerated REPowerEU plan, advanced rechargeable batteries are critical to achieving green energy systems and ensuring energy security. By 2050, Europe's demand for battery production could increase by 3500%, necessitating new recycling facilities to reduce reliance on fluctuating global critical raw material markets. Recycling could supply 40–70% of needed battery metals from 2040 onward, but immediate investment is vital to build a comprehensive European battery recycling industry. Effective waste management is also crucial to transforming waste into valuable energy resources.

In such scenario, this study presents a novel approach by utilizing PVB as a binder for HC, aiming to address critical challenges in the development of sustainable but robust and high-performing HC-based anodes for commercial LIBs and NIBs. Initially, commercial PVB was tested to determine the optimal composition, followed by using recycled PVB sourced from automotive glass waste via a patented mechanochemical process. The results demonstrate that electrodes bound with a PAA/PVB

mixture exhibit superior rate capability and high ICE in both LIB and NIB laboratory-scale battery cells, surpassing the performance of those with other binders tested. This work not only advances the performance of HC in energy storage but also provides a sustainable solution for converting waste materials into high-value-added, high-performance components, contributing to both battery technology innovation and environmental sustainability in a circular economy perspective.

4. Experimental Section

Electrodes Preparation and Li/Na Cell Assembly: All the polymers used as binder were purchased from Sigma–Aldrich: PVDF (M_w = 534000 g mol^{-1}), PAA (M_w = 450000 g mol^{-1}), and PVB (M_w = 135600 g mol^{-1}). For electrode preparation, solutions were made dissolving either PVDF or PVDF/PVB blend (80/20 mass ratio) in N-methylpyrrolidone (NMP), and PAA only, or PAA/PVB (80/20), or PAA/PVB (50/50) in ethanol, upon proper stirring till clearness. HC (hard carbon) active material (Kuranode Type 5 µm, Kuraray, Japan) and conductive carbon (Super C65, Timcal) were dry-mixed and ground. This blend was then incorporated into the prepared solutions, resulting in slurries with an active material:Super C65:binder mass ratio of 90:5:5. Stirring continued for 6 h without heating, in very mild conditions to avoid the formation of bubbles and allow the uniform dispersion of the components, which were then cast onto aluminum or copper current collector foils for NIBs or LIBs, respectively, by using a doctor blade to ensure a consistent film thickness (200 µm wet thickness) and then dried at 80 °C. The laminates were pressed and subjected to a second drying step under vacuum overnight at 120 °C (the areal active mass loading in electrodes were up to 4 mg cm^{-2}, with ≈150 µm dry thickness). For comparison, all electrodes, regardless of the binder used, were prepared with the same thickness and a solid content of 20% to ensure consistency in the evaluation.

The electrodes were transferred into a glove box (Jacomex GP concept) with water and oxygen levels below 0.9 ppm for assembling Swagelok-type 3-electrode cells. Sodium metal (Sigma–Aldrich) was used as both the counter and reference electrodes for NIBs, while lithium metal (Sigma–Aldrich) served the same purpose for LIBs. For all cells, glass fiber (Whatman GF/A) was employed as the separator. Electrolytes used were 1 M NaFSI in a 1:1 v/v mixture of ethylene carbonate (EC) and dimethyl carbonate (DMC), preformulated by E-lyte Innovations (Germany) for NIBs, and 1 M $LiPF_6$ in a 1:1 v/v mixture of EC and DMC, preformulated by Solvionic (France), for LIBs. After assembly, the cells were removed from the glove box for electrochemical testing.

Electrochemical Characterization: The long-term cycling performance of the electrodes was evaluated using a constant current-constant voltage (CC-CV) protocol with 1C equal to 300 mA g^{-1}, with respect to the HC active material mass, within a voltage (E) range of 0.01–1.5 V, using a BT-2000 battery testing system (Arbin, USA). The response of electrode films at various current densities was further examined with a C-rate capability protocol. The current rate began at C/20 and increased every five cycles up to 2C (C/20, C/10, C/5, C/2, 1C, and 2C), followed by a return to C/20. Cyclic voltammetry (CV) studies were performed at a scan rate of 0.05 mV s^{-1}, using a VMP-3 multichannel potentiostat (Biologic, France). Additionally, to better understand the Na storage characteristics related to surface capacitive and bulk diffusive behaviors, CV was recorded at various scan rates between 0.05 and 5 mV s^{-1}.

Electrochemical impedance spectroscopy (EIS) was performed after the first cycle and then at every ten cycles at a voltage of 0.5 V to evaluate the interfacial behavior of the anodes based on different binders. The measurements were conducted on the VMP-3 potentiostat with an AC amplitude of 5 mV over a frequency range of 300 kHz to 5 mHz. RelaxIS software (RHD instruments, Germany) was utilized to fit the EIS data. To evaluate the diffusion behavior, galvanostatic intermittent titration technique (GITT) measurements were conducted at a C/10 rate, with a pulse time of 20 min followed by a relaxation period of 3 h. According to Fick's second law of diffusion, the diffusion coefficient of Na^+ (D_{Na+}) can be determined as follows (for simplification in computations, it was assumed to remain constant throughout the process, and it was calculated according to the parallelepiped geometry of a thin film, $V = S{\cdot}L$):[35]

$$D = \frac{4L^2}{\pi\tau}\left(\frac{\Delta E_s}{\Delta E_\tau}\right)^2 \quad (1)$$

where τ is the pulse duration, L stands for the thickness of the electrode material, ΔE_s denotes the voltage fluctuation when the system was at rest (no current flow), and ΔE_τ signifies the voltage shift observed during a current pulse. These parameters can be derived from GITT curve for each current increment.

SEI Analysis and Morphological Characterization: The surface composition and structure of the solid electrolyte interphase (SEI) layer on HC anodes with different binders were investigated using X-ray photoelectron spectroscopy (XPS) and transmission electron microscopy (TEM). These analyses were performed on HC electrodes recovered from cells immediately after 10 cycles at 1C. Cells were opened inside the Ar-filled glove box, and the electrodes were rinsed using DMC for 10 s before examination. XPS analyses were conducted using a PHI 5000 VersaProbe instrument from ULVAC-PHI (Physical Electronics Inc., Kanagawa, Japan). Two distinct pass energy values were applied, *viz.* 187.75 and 23.5 eV for the survey and the high-resolution (HR) spectra, respectively. Throughout the measurements, charge compensation was achieved through a combination of an electron beam and a low-energy Ar beam system. A Talos F200X (Thermo Scientific) was used for TEM analysis, equipped with a Field Emission Gun (FEG) emitter and operated at an accelerating voltage of 200 kV. Additionally, SEM measurements were performed using a Benchtop SEM (JCM-6000Plus, Jeol) to investigate the morphologies of HC electrodes produced using the different binders.

Supporting Information

Supporting Information is available from the Wiley Online Library or from the author.

Acknowledgements

The SUNRISE project (https://sunrise-project.eu/) has received funding from the European Union's Horizon 2020 Research and Innovation Program under grant agreement No 958243. This study was carried out within the MOST—Sustainable Mobility Center and received funding from the European Union Next-GenerationEU (PIANO NAZIONALE DI RIPRESA E RESILIENZA—PNRR e MISSIONE 4 COMPONENTE 2, INVESTIMENTO 1.4 e D.D. 1033 June 17, 2022, CN00000023, Spoke 13). This manuscript reflects only the authors' views and opinions, and neither the European Union nor the European Commission can be considered responsible for them. Authors acknowledge support under the MUR program 'Dipartimenti di Eccellenza 2023–2027" (CUPE17G22001490006). A.P. gratefully acknowledges the Italian Ministry for University and Research (MUR) for funding under the D.M. 1062/2021 program. Authors acknowledge support under the MUR program "Dipartimenti di Eccellenza 2023–2027" (CUPE17G22001490006).

Open access publishing facilitated by Politecnico di Torino, as part of the Wiley - CRUI-CARE agreement.

Conflict of Interest

The authors declare no conflict of interest.

Data Availability Statement

The data that support the findings of this study are available on request from the corresponding author. The data are not publicly available due to privacy or ethical restrictions.

Keywords

binder, hard carbon, Li-ion battery, Na-ion battery, PVB, recycling

Received: December 31, 2024
Revised: February 10, 2025
Published online: March 3, 2025

[1] H. Wang, S. T. Liu, C. Lei, H. R. Qiu, W. Q. Jiang, X. J. Sun, Y. Q. Zhang, W. X. He, *Electrochim. Acta* **2024**, *477*, 143812.
[2] H. Darjazi, M. Falco, F. Colò, L. Balducci, G. Piana, F. Bella, G. Meligrana, F. Nobili, G. A. Elia, C. Gerbaldi, *Adv. Mater.* **2024**, *34*, 2313572.
[3] P. Desai, J. Huang, D. Foix, J. M. Tarascon, S. Mariyappan, *J. Power Sources* **2022**, *551*, 232177.
[4] S. Wu, H. Peng, L. Huang, Y. Liu, Y. Wu, L. Liu, W. Ai, Z. Sun, *Inorg. Chem. Front.* **2023**, *10*, 5908.
[5] Y. Chen, F. Li, Z. Guo, Z. Song, Y. Lin, W. Lin, L. Zheng, Z. Huang, Z. Hong, M. M. Titirici, *J. Power Sources* **2023**, *557*, 232534.
[6] C. Constable, F. Coowar, M. Copley, E. Kendrick, C. Dancer, I. Hasa, *J. Electrochem. Soc.* **2024**, *171*, 023506.
[7] M. S. Balogun, Y. Luo, W. Qiu, P. Liu, Y. Tong, *Carbon N Y* **2016**, *98*, 162.
[8] M. Bartoli, A. Piovano, G. A. Elia, G. Meligrana, R. Pedraza, N. Pianta, C. Tealdi, G. Pagot, E. Negro, C. Triolo, L. V. Gomez, N. Comisso, A. Tagliaferro, S. Santangelo, E. Quartarone, V. Di Noto, P. Mustarelli, R. Ruffo, C. Gerbaldi, *Renewable Sustainable Energy Rev.* **2024**, *194*, 114304.
[9] L. Liu, L. Xiao, Z. Sun, S. Bashir, R. Kasi, Y. Gu, R. Subramaniam, *J. Energy Chem.* **2024**, *94*, 414.
[10] Y. Chu, J. Zhang, Y. Zhang, Q. Li, Y. Jia, X. Dong, J. Xiao, Y. Tao, Q. H. Yang, *Adv. Mater.* **2023**, *35*, 2212186.
[11] L. Xie, C. Tang, Z. Bi, M. Song, Y. Fan, C. Yan, X. Li, F. Su, Q. Zhang, C. Chen, *Adv. Energy Mater.* **2021**, *11*, 2101650.
[12] D. A. Stevens, J. R. Dahn, *J. Electrochem. Soc.* **2000**, *147*, 1271.
[13] Z. Tang, R. Zhang, H. Wang, S. Zhou, Z. Pan, Y. Huang, D. Sun, Y. Tang, X. Ji, K. Amine, M. Shao, *Nat. Commun.* **2023**, *14*, 6024.
[14] Z. Song, F. Li, L. Mao, W. Lin, L. Zheng, Y. Huang, M. Wei, Z. Hong, *ACS Sustain Chem Eng* **2023**, *11*, 15020.
[15] D. Alvira, D. Antorán, H. Darjazi, G. A. Elia, C. Gerbaldi, V. Sebastian, J. J. Manyà, *J Mater Chem A Mater* **2025**, *13*, 2730.
[16] Y. Zhen, R. Sa, K. Zhou, L. Ding, Y. Chen, S. Mathur, Z. Hong, *Nano Energy* **2020**, *74*, 104895.
[17] J. L. Xia, A. H. Lu, X. F. Yu, W. C. Li, *Adv. Funct. Mater.* **2021**, *31*, 2104137.
[18] C. Bak, K. G. Kim, H. Lee, S. Byun, M. Lim, H. An, Y. Roh, J. Lim, C. B. Dzakpasu, D. Kim, J. Lee, H. Lee, H. Lee, Y. M. Lee, *Chem. Eng. J.* **2024**, *483*, 148913.
[19] H. Yoon, P. Behera, S. Lim, T. G. Yun, B. Hwang, J. Y. Cheong, *Int. J. Energy Res.* **2024**, *2024*, 8893580.
[20] L. El Ouatani, R. Dedryvère, J. B. Ledeuil, C. Siret, P. Biensan, J. Desbrières, D. Gonbeau, *J. Power Sources* **2009**, *189*, 72.
[21] S. Trivedi, V. Pamidi, S. P. Bautista, F. N. A. Shamsudin, M. Weil, P. Barpanda, D. Bresser, M. Fichtner, *Adv. Energy Mater.* **2024**, *14*, 26.
[22] H. Darjazi, A. Staffolani, L. Sbrascini, L. Bottoni, R. Tossici, F. Nobili, *Energies* **2020**, *13*, 6216.
[23] W. Li, X. Guo, K. Song, J. Chen, J. Zhang, G. Tang, C. Liu, W. Chen, C. Shen, *Adv. Energy Mater.* **2023**, *13*, 2300648.
[24] J. Jiao, C. Yi, X. Qiu, D. Yang, F. Fu, W. Liu, *Green Chem.* **2024**, *26*, 6643.
[25] R. Wang, L. Feng, W. Yang, Y. Zhang, Y. Zhang, W. Bai, B. Liu, W. Zhang, Y. Chuan, Z. Zheng, H. Guan, *Nanoscale Res. Lett.* **2017**, *12*, 575.
[26] R. Wang, L. Feng, W. Yang, Y. Zhang, Y. Zhang, W. Bai, B. Liu, W. Zhang, Y. Chuan, Z. Zheng, H. Guan, *Nanoscale Res. Lett.* **2017**, *12*, 575.
[27] Q. Fan, W. Zhang, J. Duan, K. Hong, L. Xue, Y. Huang, *Electrochim. Acta* **2015**, *174*, 970.
[28] L. Chen, K. Song, J. Shi, J. Zhang, L. Mi, W. Chen, C. Liu, C. Shen, *Sci. China Mater.* **2021**, *64*, 105.
[29] I. Cho, S. Gong, D. Song, Y. G. Lee, M. H. Ryou, Y. M. Lee, *Sci. Rep.* **2016**, *6*, 30945.
[30] R. Dachowski, P. Kostrzewa, *Procedia Eng* **2016**, *161*, 754.
[31] X. Zhang, H. Hao, Y. Shi, J. Cui, *Constr. Build. Mater.* **2015**, *93*, 404.
[32] L. Calucci, S. Pizzanelli, A. Mandoli, A. Birczyński, Z. T. Lalowicz, C. De Monte, L. Ricci, S. Bronco, *Polymers* **2021**, *13*, 2686.
[33] S. Porporato, H. Darjazi, M. Gastaldi, A. Piovano, A. Perez, B. Yécora, A. Fina, G. Meligrana, G. A. Elia, C. Gerbaldi, *Adv. Sustainable Syst.* **2025**, *9*, 2400569.
[34] F. Lian, Y. Wen, Y. Ren, H. Guan, *J Memb Sci* **2014**, *456*, 42.
[35] D. Alvira, D. Antorán, J. J. Manyà, *J. Energy Chem.* **2022**, *75*, 457.
[36] Y. Li, M. P. Paranthaman, K. Akato, A. K. Naskar, A. M. Levine, R. J. Lee, S. O. Kim, J. Zhang, S. Dai, A. Manthiram, *J. Power Sources* **2016**, *316*, 232.
[37] A. Urbanski, A. Omar, J. Guo, A. Janke, U. Reuter, M. Malanin, F. Schmidt, D. Jehnichen, M. Holzschuh, F. Simon, K.-J. Eichhorn, L. Giebeler, P. Uhlmann, *J. Electrochem. Soc.* **2019**, *166*, A5275.
[38] S. Alvin, H. S. Cahyadi, J. Hwang, W. Chang, S. K. Kwak, J. Kim, *Adv. Energy Mater.* **2020**, *10*, 2000283.
[39] Z. Guo, Z. Xu, F. Xie, J. Jiang, K. Zheng, S. Alabidun, M. Crespo-Ribadeneyra, Y. S. Hu, H. Au, M. M. Titirici, *Adv. Mater.* **2023**, *35*, 2304091.
[40] J. Wang, L. Xi, C. Peng, X. Song, X. Wan, L. Sun, M. Liu, J. Liu, *Adv. Eng. Mater.* **2024**, *26*, 2302063.
[41] Y. Zhen, Y. Chen, F. Li, Z. Guo, Z. Hong, M.-M. Titirici, *Proc. Natl. Acad. Sci. USA* **2021**, *118*, 2111119118.
[42] Y. Huang, Y. Wang, P. Bai, Y. Xu, *ACS Appl. Mater. Interfaces* **2021**, *13*, 38441.
[43] Y. Chen, F. Li, Z. Guo, Z. Song, Y. Lin, W. Lin, L. Zheng, Z. Huang, Z. Hong, M. M. Titirici, *J. Power Sources* **2023**, *557*, 232534.
[44] H. Darjazi, L. Bottoni, H. R. Moazami, S. J. Rezvani, L. Balducci, L. Sbrascini, A. Staffolani, A. Tombesi, F. Nobili, *Materials Today Sustainability* **2023**, *21*, 100313.
[45] D. Alvira, D. Antorán, H. Darjazi, G. A. Elia, V. Sebastian, J. J. Manyà, *J. Power Sources* **2024**, *614*, 235043.
[46] S. Lin, H. Zhang, C. Shu, W. Hua, X. Wang, Y. Zhao, J. Luo, Z. Tang, Y. Wu, W. Tang, *Adv. Funct. Mater.* **2024**, *34*, 2409628.
[47] N. Elgrishi, K. J. Rountree, B. D. McCarthy, E. S. Rountree, T. T. Eisenhart, J. L. Dempsey, *J. Chem. Educ.* **2018**, *95*, 197.
[48] G. Yang, X. Li, Z. Guan, Y. Tong, B. Xu, X. Wang, Z. Wang, L. Chen, *Nano Lett.* **2020**, *20*, 3836.
[49] A. Nytén, M. Stjerndahl, H. Rensmo, H. Siegbahn, M. Armand, T. Gustafsson, K. Edström, J. O. Thomas, *J. Mater. Chem.* **2006**, *16*, 3483.
[50] M. Hekmatfar, A. Kazzazi, G. G. Eshetu, I. Hasa, S. Passerini, *ACS Appl. Mater. Interfaces* **2019**, *11*, 43166.
[51] N. Qin, Y. Sun, C. Hu, S. Liu, Z. Luo, X. Cao, S. Liang, G. Fang, *J. Energy Chem.* **2023**, *77*, 310.
[52] R. Dedryvère, S. Laruelle, S. Grugeon, P. Poizot, D. Gonbeau, J.-M. Tarascon, *Chem. Mater.* **2004**, *16*, 1056.
[53] J. Fondard, E. Irisarri, C. Courrèges, M. R. Palacin, A. Ponrouch, R. Dedryvère, *J. Electrochem. Soc.* **2020**, *167*, 070526.
[54] M. Ma, H. Cai, C. Xu, R. Huang, S. Wang, H. Pan, Y. S. Hu, *Adv. Funct. Mater.* **2021**, *31*, 2100278.
[55] V. Nikitakos, A. D. Porfyris, K. Beltsios, C. Papaspyrides, S. Bordignon, M. R. Chierotti, S. Nejrotti, M. Bonomo, C. Barolo, A. Piovano, R. Pfaendner, B. Yecora, A. Perez, *Polymers* **2023**, *16*, 10.

[56] J. Fondard, E. Irisarri, C. Courrèges, M. R. Palacin, A. Ponrouch, R. Dedryvère, *J. Electrochem. Soc.* **2020**, *167*, 070526.
[57] Y. Huang, Y. Wang, P. Bai, Y. Xu, *ACS Appl. Mater. Interfaces* **2021**, *13*, 38441.
[58] L. Xie, C. Tang, Z. Bi, M. Song, Y. Fan, C. Yan, X. Li, F. Su, Q. Zhang, C. Chen, *Adv. Energy Mater.* **2021**, *11*, 2101650.
[59] N. LeGe, X.-X. He, Y.-X. Wang, Y. Lei, Y.-X. Yang, J.-T. Xu, M. Liu, X. Wu, W.-H. Lai, S.-L. Chou, *Energy Environ. Sci.* **2023**, *16*, 5688.
[60] L. Bottoni, H. Darjazi, L. Sbrascini, A. Staffolani, S. Gabrielli, G. Pastore, A. Tombesi, F. Nobili, *ChemElectroChem* **2023**, *10*, 202201117.
[61] N. Cei, I. Canesi, S. Nejrotti, G. Montalbano, H. Darjazi, A. Piovano, M. Bonomo, A. Fina, B. Yecora, A. Perez, C. Barolo, C. Gerbaldi, D. Spinelli, *Polymers* **2024**, *16*, 3439.
[62] C. F. Acevedo, L. Martínez De Morentín Osaba, E. Osés Arteta, G. M. Herrera, M. A. Fernández Fernández, Polyvinyl Butyral Recycling Method Patent EP2308919A1 **2011**.